ADVANCED FUNCTIONAL MATERIALS
www.afm-journal.de

www.MaterialsViews.com

Controlling Polymorphism in Poly(3-Hexylthiophene) through Addition of Ferrocene for Enhanced Charge Mobilities in Thin-Film Transistors

*Brandon H. Smith, Michael B. Clark Jr., Hao Kuang, Christopher Grieco, Alec V. Larsen, Chenhui Zhu, Cheng Wang, Alexander Hexemer, John B. Asbury, Michael J. Janik, and Enrique D. Gomez**

Crystalline organic molecules often exhibit the ability to assemble into multiple crystal structures depending on the processing conditions. Exploiting this polymorphism to optimize molecular orbital overlap between adjacent molecules in the unit lattice is an effective method for improving charge transport within the material. In this study, grazing incident X-ray diffraction was employed to demonstrate the formation of tighter π-π stacking poly(3-hexylthiophene-2,5-diyl) polymorphs in films spin coated from ferrocene-containing solutions. As a result, the addition of ferrocene to casting solutions yields thin-film transistors which exhibit approximately three times higher source-drain currents and charge mobilities than neat polymer devices. Nevertheless, XPS depth profiling and NMR analyses of the active layer reveal that all ferrocene is removed during the spin coating process, which may be an essential factor to achieve high mobilities. Such insights gleaned from ferrocene/poly(3-hexylthiophene-2,5-diyl) mixtures can serve as a template for selection and optimization of other small molecule/polymer systems with greater baseline charge mobilities.

1. Introduction

The development of polymer semiconductors such as polyacetylene and polythiophene in the 1970s represents one of the decisive early efforts in the field of organic electronics.[1] A decade later, the development of soluble polythiophene derivatives exhibiting significant charge transport broadened the scope of potential applications.[2] At approximately the same time, the first organic thin-film transistors (OTFTs) were reported.[3] The subsequent merger of thin-film transistor technology with high performance, soluble polythiophene active layers would eventually enable the fabrication of organic devices exhibiting charge mobilities exceeding 1 $cm^2 V^{-1} s^{-1}$, which rival that of commercially available hydrogenated amorphous silicon transistors (a-Si:H).[4,5]

Despite major advances, simple, effective, and economical methods for further increasing the performance of semiconducting polymers must be identified. The path to widespread commercialization of OTFTs is replete with impediments, and in order for OTFTs to fully compete with and even exceed inorganic counterparts, the commonly expounded advantages associated with cost-friendly solution processing, large area printing techniques, and flexible devices must also be accompanied by impressive low-bias source-drain current, on/off ratio, and charge mobility characteristics.[6,7] While other types of higher mobility organic materials, such as organic small molecules and single crystals, have garnered significant attention in recent years, the challenges encountered in the realms of processing, fabrication, and stability limit their appeal for large volume production.[6,8,9] Consequently, polymer-based transistors seem to offer an attractive route to ubiquitous organic field-effect transistor (OFET) implementation.[10]

One of the principal challenges associated with the development of OFETs is the enhancement of charge mobilities. Designing materials capable of supporting high charge mobilities requires intricate control of the charge transfer integrals within crystalline phases.[11,12] Weak van der Waals intermolecular forces in organics, however, lead to a rough free energy landscape and multiple metastable polymorphs in many cases.[13] As a consequence, access to various crystal structures of the same organic molecule is possible through the use of additives or manipulation of the processing conditions.[14,15] Because polymorphs can possess significantly different charge

B. H. Smith, H. Kuang, Prof. M. J. Janik, Prof. E. D. Gomez
Department of Chemical Engineering
The Pennsylvania State University
University Park
Pennsylvania, 16802, USA
E-mail: edg12@psu.edu
Dr. M. B. Clark Jr.,
The Dow Chemical Company
Collegeville, Pennsylvania, 19426, USA
C. Grieco, A. V. Larsen, Prof. J. B. Asbury
Department of Chemistry, The Pennsylvania State University
University Park
Pennsylvania, 16802, USA
Dr. C. Zhu, Dr. C. Wang, Dr. A. Hexemer
Advanced Light Source, Lawrence Berkeley National Laboratory
Berkeley, California, 94720, USA

DOI: 10.1002/adfm.201403089

mobilities, navigating the complex free energy landscape of organic and polymeric materials is crucial to achieve high performance devices.

Work conducted by Troisi and Orlandi has illustrated the potential benefits of polymorph-selective processing with regards to charge transport in pentacene devices by comparing the band structure of each of the four known crystal types and identifying the best form for use in OTFTs.[16] Commonly reported techniques employed to induce preferential crystallization of certain polymorphs include solvent and thermal annealing, substrate confinement, substrate modification, deposition temperature control, pressure, and solution shear.[15,17] Polymer-mediated control has also been described for 6,13-bis(triisopropylsilyleth ynyl)pentacene (TIPS-pentacene) at a 1:1 ratio by weight with poly(3-hexylthiophene-2,5-diyl) (P3HT), yielding roughly nine times greater mobility than the neat small molecule.[18] A study conducted by Chen et al. revealed a correlation between the type of solvent employed and the resulting crystal structure for the small molecule 5,11-bis(triethylsilylethynyl)anthradithiophene (TES ADT). A new polymorph was generated by slow crystallization from a weakly polar solvent, and device performance increased approximately ten-fold over the known structure.[17] Research performed by the Loo group has developed a post-processing method whereby annealing under various solvents prompted crystallization into one of two types of hexabenzocoronene (HBC) polymorphs. The HBC molecules crystallized from good solvents formed herringbone-like structures, exhibiting greater hydrogen bonding potentials and smaller molar volumes, but crystallization from poor solvents with small hydrogen bonding potentials and large molar volumes resulted in a slip-stacked structure.[19]

In this paper, we present an approach to control the polymorphism in poly(3-hexylthiophene-2,5-diyl) (P3HT) utilized as TFT active layers and thereby enhance charge mobilities in devices. We demonstrate that the presence of ferrocene (Fc) at intermediate to high concentrations in P3HT casting solutions prepared with trichlorobenzene (TCB) as a solvent yields devices exhibiting significantly greater source-drain current and charge mobilities than neat P3HT devices. The observed enhancement effect scales roughly linearly with increasing ferrocene content up to very high ferrocene concentrations in solution (>9:1 ferrocene:P3HT by weight), at which point, film inhomogeneity becomes an important limitation.

2. Results and Discussion

The compositions of thin films spin coated from ferrocene-containing P3HT solutions were examined at each stage of the transistor fabrication process. In addition to ferrocene, a ferrocene derivative containing large substituent groups designated 1,1′-bis(di-tert-butylphosphino)ferrocene (BTBP Fc) was also investigated. Surprisingly, the amount of small molecule deposited during spin-coating depends on whether solutions contained Fc or BTBP Fc.

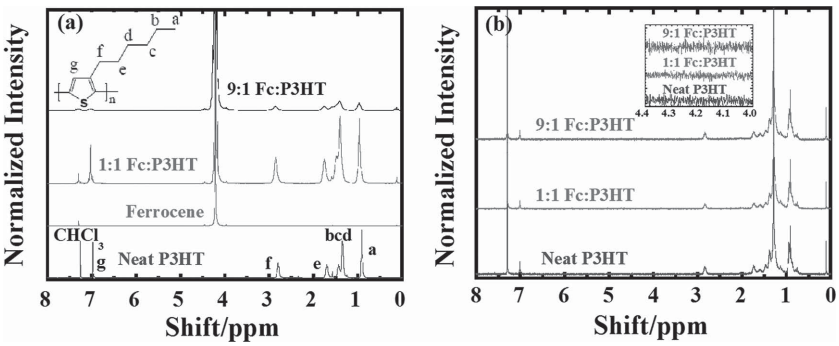

Figure 1. ^{1}H NMR analysis of a) Fc:P3HT $CDCl_3$ solutions and b) thin films spun cast from Fc:P3HT solutions onto untreated Si wafers and re-dissolved in $CDCl_3$. Inset for (b) provides a zoomed view of the ferrocene region of interest. Scans have been normalized and baseline offset for clarity.

Ferrocene concentrations were ascertained from nuclear magnetic resonance (NMR) spectroscopy for Fc:P3HT solutions and films cast from 9:1 Fc:P3HT solutions. Ferrocene and P3HT concentrations obtained by integrating the ferrocene peak at 4.2 ppm and the P3HT peak at ≈2.8 ppm of **Figure 1**a were quantitatively equivalent to the expected solution concentrations. Ferrocene contents of 45 and 89 wt% of total solids were estimated from NMR results, compared to expected concentrations of 51 and 91 wt% Fc. Figure 1b displays results for five films which were spin coated from each solution onto three inch diameter untreated silicon wafers, re-dissolved in deuterated chloroform, and combined for the NMR measurement. These films were not annealed or exposed to vacuum in an attempt to eliminate all potential avenues for ferrocene sublimation. Nevertheless, NMR measurements for the re-dissolved films showed that ferrocene was not present in the film after spin coating at any appreciable concentration.

Solutions and films for Fc:P3HT and BTBP Fc:P3HT were also analyzed with UV–Vis absorbance spectroscopy (Figure S1, Supporting Information). Ferrocene concentrations obtained by fitting the solution absorbances were in close agreement with targeted values based on the dispensed mass of each solid. For as-cast films, however, the Fc:P3HT spectra perfectly overlaid that of neat P3HT when normalized to account for minor film thickness variations. Unlike BTBP Fc:P3HT films, the absorbance specific to the metallocene in the 300–350 nm region was not visible in Fc:P3HT films, suggesting that most of the ferrocene was lost during the spin coating process. Moreover, analysis of thermally annealed films and with X-ray photoelectron spectroscopy (XPS) depth profiles confirm that all detectable ferrocene was removed from the spin cast film during the fabrication process, yet ferrocene remains in unannealed drop cast films (Figure S2, Supporting Information). The results collectively indicate that ferrocene leaves with the solvent during the spin coating process. This is perhaps due to the similar molecular weights of ferrocene and TCB (186.0 g mol^{-1} vs 181.5 g mol^{-1}), despite the large differences between the vapor pressures (1.0 Pa vs 38.7 Pa at 298 K, respectively).[20]

Structural and morphological properties for thin films prepared from multiple compositions of Fc:P3HT and BTBP

Fc:P3HT solutions were investigated through X-ray scattering experiments. P3HT films have been shown to adopt a microcrystalline lamellar microstructure consisting of 2-dimensional conjugated layers with strong π–π interchain interactions separated by the solubilizing, insulating alkyl chains.[21] As a result, charge transport is anisotropic and favored along the in-plane π-stacking direction parallel to the conjugated sheets.[22,23] The (100), (200), and (300) P3HT diffraction peaks correspond to the out-of-plane spacing between the backbones of the polymer through the alkyl side chains, and the (020) reflection is associated with the in-plane π–π stacking between chains.[21,24] When the out-of-plane reflections are most intense at the meridian, the chains are primarily oriented with the (100) plane parallel to the substrate in an "edge-on" configuration, as opposed to the "face-on" ordering in which the (100) plane is normal to the substrate surface.[22,25] Prior work has demonstrated that highly regioregular P3HT preferentially aligns in an "edge-on" manner with the side chains standing upright on the insulator surface.[6]

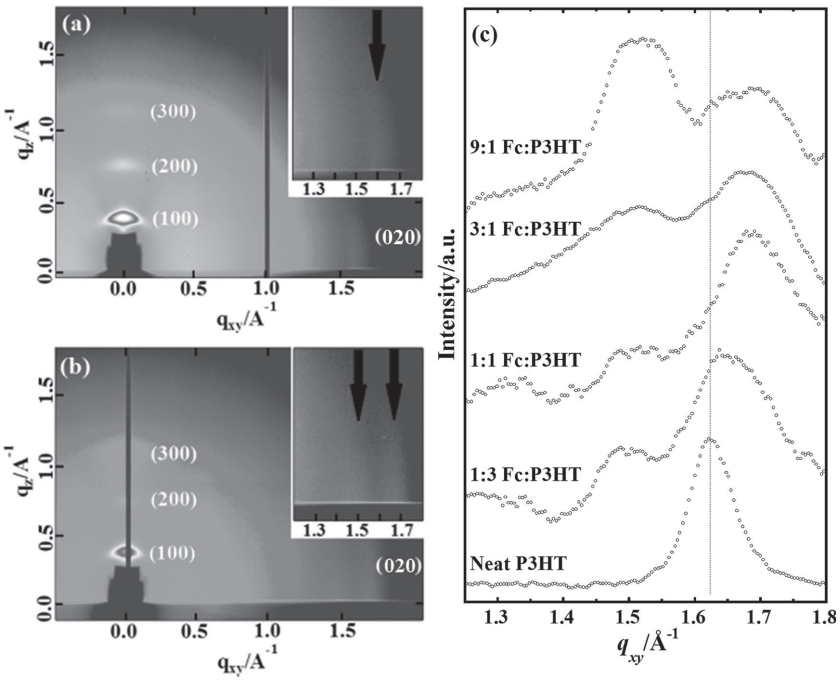

Figure 2. 2-D grazing-incidence X-ray diffraction images for films spun cast from a) P3HT and b) 3:1 Fc:P3HT solutions. Insets provide a close-up view of the (020) region of interest with arrows identifying peak locations. c) Profiles of the (020) region of interest for films spun cast from P3HT/ferrocene solutions. All films were annealed at 150 °C under an N_2 atmosphere.

Rocking curves were obtained around the P3HT (100) reflection to investigate the crystallinity (Figure S3a, b, Supporting Information),[26] and grazing incidence X-ray diffraction (GIXRD) was employed to analyze the in-plane ordering from the (020) peak. From the rocking curves, we observed similar d-spacing for both sets of blends (d_{100} = 16.0 ± 0.2 Å), but the samples containing BTBP Fc exhibited a slightly increasing trend with interchain spacing growing from 15.9 to 16.2 Å. The degree of crystallinity is proportional to the integral of the rocking curve intensity. As such, relative crystallinity and orientation estimates were acquired by integrating the rocking curves over the azimuthal direction. Little change is observed with increasing ferrocene content for Fc:P3HT samples (Figure S3c, Supporting Information). Conversely, the relative crystallinity of the 9:1 BTBP Fc:P3HT film suffered a 40% decrease (Figure S3d, Supporting Information), presumably a consequence of the high concentration of BTBP Fc molecules.

Analysis of the P3HT (020) reflection from GIXRD of films revealed that the in-plane spacing decreases with increasing ferrocene concentration in solution but remains constant regardless of BTBP Fc content. In **Figure 2**, the (020) peak position near 1.62 $Å^{-1}$ shifts towards higher q_{xy} values indicating the d_{020}-spacing changed from ≈3.88 Å, which is consistent with values reported for neat P3HT films, to roughly 3.82, 3.76, 3.74, and 3.72 Å for films from 1:3, 1:1, 3:1, and 9:1 Fc:P3HT solutions, respectively.[27–29] Furthermore, a reflection at 1.51 $Å^{-1}$ becomes visible when ferrocene is included in solutions prior to spin-coating, and the intensity of this reflection increases with ferrocene solution content. The feature at 1.51 $Å^{-1}$ does not correspond to any of the reported crystal structures for P3HT.[21,30] Films spin coated from BTBP Fc:P3HT solutions, in contrast, demonstrated neither the (020) peak shift nor the reflection at 1.51 $Å^{-1}$, as illustrated in Figure S4, Supporting Information.

The observed alteration of the P3HT unit cell due to interactions with ferrocene during spin coating is best described in terms of polymorphism, where the polymer adopts different crystalline structures depending on the solvent, annealing temperature, and processing conditions.[31] Analogous polymorphic behavior in poly(3-alkylthiophenes) has been demonstrated, and two distinct P3HT forms, designated Form I and II, are well established and characterized. Form I is obtained after rapid solvent evaporation, and it exhibits a unit cell with spacing through the non-interdigitated side chains (*a*-axis) of 16 Å and spacing between layers (*b*/2) of 3.8 Å.[32] Form II is generated from very slow solvent evaporation processes, and as such, is less commonly reported than Form I. The Form II unit cell is comprised of a shorter *a*-axis resulting from tilted and interdigitated alkyl chains, but the *b*-axis length increases due to the packing tendencies of the long alkyl segments.[27,33] A metastable Form I′ with wider π–π spacing due to more extended, non-interdigitated side chains has also been observed after extremely slow solvent evaporation at low temperatures (i.e., 13 °C for 24 h).[28] The unit cell dimensions of known P3AT polymorphs are compared with those of the new ferrocene-induced Form III in **Table 1**.

In the cases of Form I′ and II P3HT polymorphs, the decreased *a*-axis with respect to Form I is accompanied by an increased π–π spacing distance. For P3HT transistors, significant interchain transport is required for charges to traverse the distance between the source and drain, so π-orbital overlap between neighboring polymer chains is a crucial limiting factor. Form I is therefore expected to possess the highest mobility

Table 1. Unit cell parameters of reported P3AT polymorphs.

Form	I[34,35]	I′[28,31]	II[27,30]	III[a)]
a/Å	16–17	15.1–15.5	11–15	16
b/Å	7.6–7.8	7.6–8.1	7.8–8.8	7.4
c/Å	7.8	7.9	9.4	—

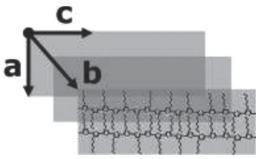

[a)]This work.

of the three types based solely on orbital overlap considerations.[34,36] Charge mobilities, however, can often be affected by the interplay between the in- and out-of-plane spacing. Paracrystalline systems incorporating other organic semiconductors, for instance, may experience detrimental effects stemming from increased separation within the *a*-axis of the unit cell, and the net effect from a shorter *b*-axis polymorph may not improve the overall charge mobility.[31] Unlike Form I′ and II, the new polymorph generated with the addition of ferrocene to P3HT spin casting solutions compressed the π–π stacking planes while maintaining a tight Form I packing of the substituent alkyl chains.

We examine the effect of compressing the π-stacking distance by measuring charge mobilities in thin film-transistors (TFTs) where the active layer is spun cast from Fc:P3HT solutions. Bottom-gate, bottom-contact TFTs were fabricated by spin coating from 10 mg P3HT mL^{-1} TCB solutions containing various ferrocene concentrations onto patterned gold source and drain electrodes on SiO_2/Si substrates. All samples were thermally annealed at 150 °C for 3 hours. In **Figure 3**, characteristics for a representative device prepared from a Fc:P3HT solution composed of 90% ferrocene and 10% P3HT by mass (9:1 Fc:P3HT, 10 mg P3HT per mL solution) are compared with those for a neat P3HT control device. The higher current observed for TFTs from 9:1 Fc:P3HT solutions is evident in Figure 3a, which shows the source-drain current (I_D) as a function of source-drain voltage (V_D) for gate voltages (V_G) ranging from –100 V to 0 V in 20 V increments. I_D increased approximately threefold from ≈1 µA for neat P3HT to ≈3 µA for the Fc:P3HT solution at a gate and source-drain bias of –100 V. No contact effects were apparent, and a similar enhancement in drain current from ≈2.5 µA to ≈6 µA is displayed in the transfer curves of Figure 3b without any substantial alteration of the threshold voltage due to the addition of ferrocene.

Charge mobilities are extracted from the transfer curve data in the saturation region. As expected for SiO_2 dielectric layers coated with hydrophobic alkyltrichlorosilanes, p-type behavior was observed; hole mobilities estimated over the I_D–V_G sweep are plotted in Figure 3c for each sample.[37] The mobility of the polymer/metallocene blend device was around two to three times higher than the neat P3HT device. Although mobilities can be overestimated due to charge injection problems (problems in charge injection are not apparent in Figure 3a),[38] taken together, the combination of higher extracted mobilities and

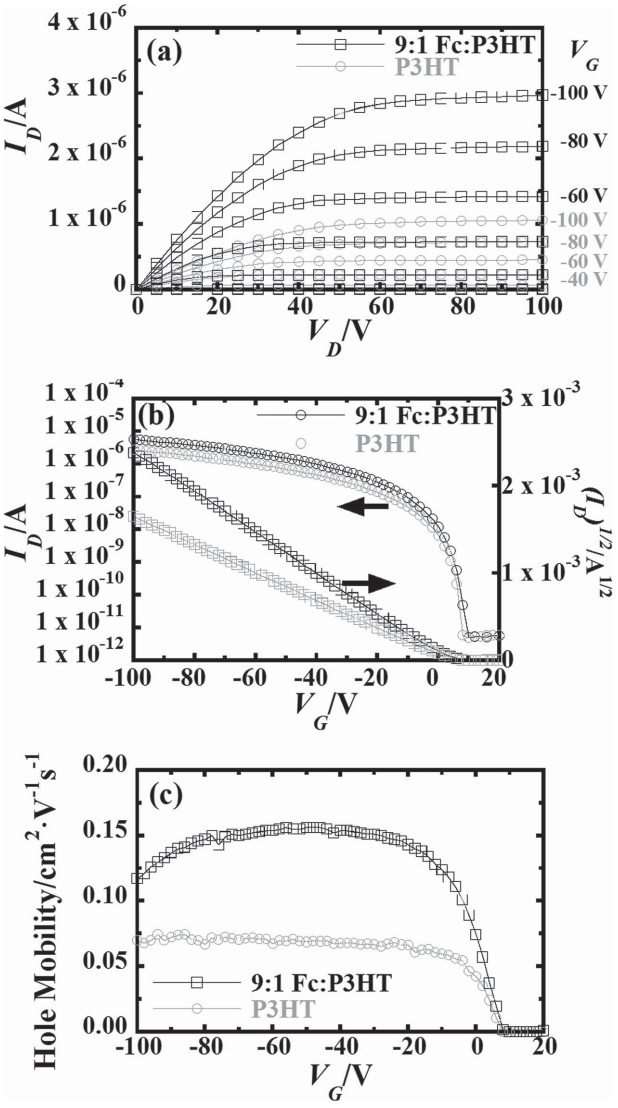

Figure 3. a) Output, b) transfer, and c) mobility plots for representative OTFTs prepared from neat P3HT and 9:1 Fc:P3HT solutions. Channel length and width dimensions are 320 and 220 µm, respectively. The dielectric layer is 300 nm of SiO_2. The source-drain bias is –100 V.

improvement in source-drain current denotes increased charge transport within Fc:P3HT devices. Several ferrocene concentrations were analyzed over the course of the study, and average values are summarized in **Figure 4**a. The highest average mobility, 0.19 cm^2 V^{-1} s^{-1}, was observed for devices made from 13:1 Fc:P3HT solutions, and the average value obtained for neat P3HT was 0.04 cm^2 V^{-1} s^{-1}. Concentrations of ferrocene at and beyond 13:1, however, lead to problems in film quality, degrading performance (Figure S5, Supporting Information). These results are averaged over five independent experiments and comprise measurements for multiple devices at each composition.

Consequently, we infer that the smaller π–π stacking distance increases molecular orbital overlap between the thiophene repeat units, thereby increasing the charge transfer integral describing the electronic wave function overlap between

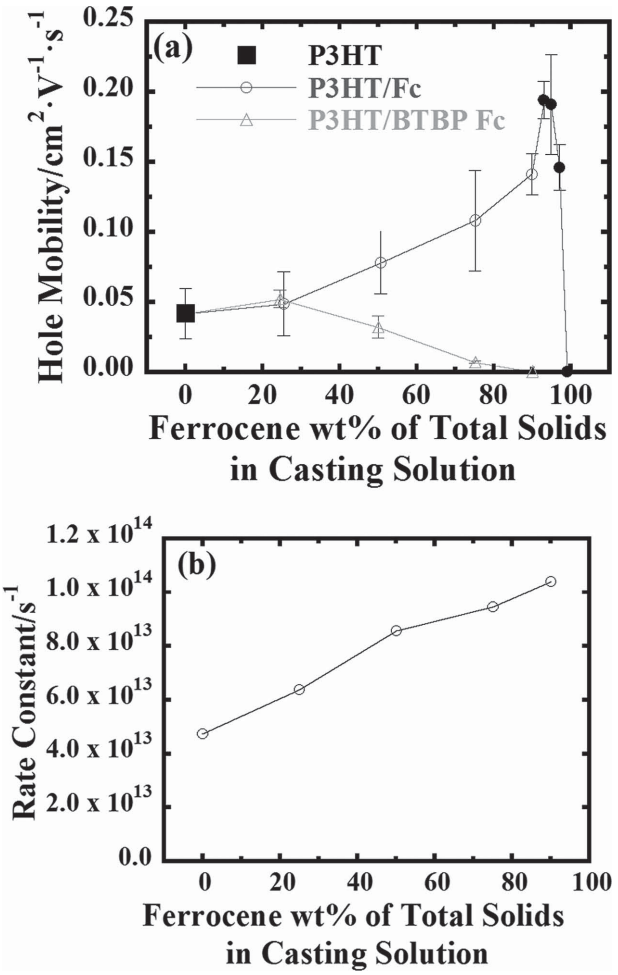

Figure 4. a) Average mobilities of TFTs prepared from P3HT/ferrocene solutions. The amount of ferrocene is given as the weight percent of total solids in the casting solutions. Dark circles represent devices made with active layers of poor film quality due to the high ferrocene content (see Figure S5, Supporting Information). Error bars indicate the standard deviation of multiple measurements averaged over five independent experiments and represent approximately 160 devices. b) Predicted values for charge transfer rate constant of sexithiophene (a model system for P3HT) at observed π-stacking distances from Figure 2.

adjacent molecules.[39] The π-stacking direction has been shown to be the primary mode for current propagation in P3HT TFTs, so decreasing the hopping distance between chain backbones significantly improves charge mobilities within the material. Density functional theory calculations were employed to quantify the expected increase in charge transfer rate constants (Figure 4b and Figure S6, Supporting Information),[40] which is proportional to charge mobilities, and the results predict an approximately two-fold increase for a 3.88 to 3.72 Å decrease in π-stacking distance.

In addition to ferrocene, we also explored the effect of blending BTBP Fc with P3HT. Solutions were prepared in the same manner as Fc:P3HT blends by mixing the polymer and metallocene for ≈14 hours. The mobilities as a function of composition presented in Figure 4a show that charge mobilities did not increase with the addition of BTBP Fc. The average mobility of devices decreased sharply with increasing BTBP Fc concentration in solution past ≈1:3 BTBP Fc:P3HT, signifying ferrocene derivatives do not universally enhance charge mobilities in P3HT.

The fact that only TFTs prepared from Fc:P3HT solutions demonstrate increasing charge mobility with increasing ferrocene supports the correlation between the short π–π stacking distances and high mobility. Ferrocene, the first metallocene originally synthesized in 1951,[41] exhibits no significant charge conduction, so the observed mobility enhancement cannot be a result of the bulk properties of ferrocene. We have also established that ferrocene is not present at detectable levels after spin coating to influence the charge transport properties (Figure 1, and Figure S1, S2, Supporting Information). The performance of solution-processed OTFTs has been shown to be highly dependent on the morphology of the active layer obtained during fabrication because the time available for polymer crystallization and film formation is very short in the spin casting process.[9,42] As such, our results indicate that the addition of ferrocene promotes the formation of a previously unreported P3HT polymorph, and the subsequent removal of the small molecule with the solvent allows for efficient charge transport through the film.

By contrast, BTBP Fc remains after spin-casting in P3HT films. UV–Vis absorption measurements confirm the presence of BTBP Fc in as-cast spin coated films and after annealing. BTBP Fc is a larger, less soluble molecule than ferrocene, which does not sublime below 150 °C. Accordingly, one explanation for the decreased charge mobilities despite constant π-stacking distances in P3HT films containing BTBT Fc is the decrease in the concentration of the P3HT phase and interruption of the conduction pathways.[43]

All indications thus far point towards the fact that ferrocene influences the nucleation of P3HT crystals early in the fabrication process. Whether ferrocene alters the nucleation process of P3HT beginning in the solution phase or the spin coating process remains unclear. One possible explanation is that ferrocene acts as nucleation centers for the polymer within the casting solution by initiating limited nucleation. These small nuclei could form with a specific crystal structure and seed larger crystals during film formation,[13,44] which then propagate with the same polymorph as the core. Evidence of increasing aggregation with ferrocene concentration supporting this conclusion has been obtained from dynamic light scattering measurements of casting solutions, provided in **Figure 5**.

It is also plausible that the metallocene's primary impact is felt during the initial stage of the spin coating process. In the wet film condition, rapid solvent removal increases the solids concentration of the forming film and commences spontaneous nucleation. Ferrocene could serve as ready nucleation centers inducing the formation of nuclei with tighter packing. Given that substituted ferrocene (BTBP-Fc) does not appear to significantly affect the crystallization of P3HT, we surmise that intermolecular interactions between the ring systems of ferrocene and conjugated backbones lead to nuclei of a polymorph with tighter π-stacking than previously reported Form I. Crystal growth from these nuclei then proceeds under the dry film condition and post-process thermal annealing.

We now consider other possible mechanisms that could explain the mobility enhancement observed with the addition of

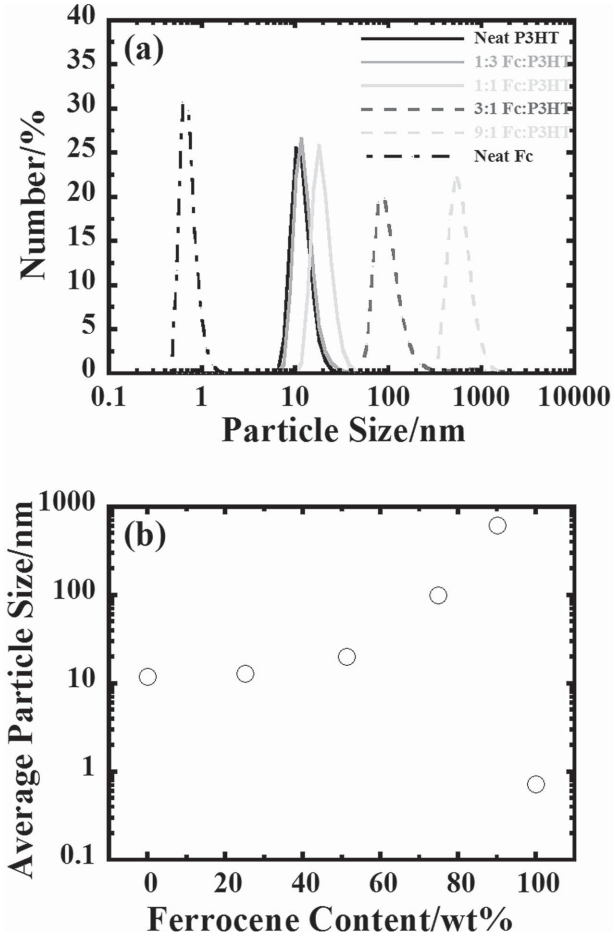

Figure 5. a) Number distributions and b) average particle sizes in Fc:P3HT solutions from dynamic light scattering measurements.

ferrocene to casting solutions. The addition of some small molecules has been proven to augment the stability of polymers by serving as excited state quenchers and radical scavengers.[45] If ferrocene acts to scavenge trap species from P3HT, the transport properties of the active layer would mark the change. Charge traps can include chemical or ionic impurities, radical moieties, structural defects and grain boundaries in the polymer, defects at the semiconductor-dielectric interface, residual surface water, and polar electrochemical trapping groups such as hydroxyls, silanols, or carbonyls.[4,46–48] Trapping entities reduce the mobile charge carrier density, so neutralization of the charge traps would be evidenced by increased overall mobilities.

The ferrocene/ferrocenium (Fc/Fc^+) system is a well-known redox couple which could serve to neutralize ionic traps or bind trapping groups while in solution.[49] In light of the fact that ferrocene is removed during spin coating, such complexation or scavenging reactions would see any impurities bound to the ferrocene and removed from the system, perhaps leaving ultrapure P3HT in the TFT conduction channel. The increasing mobility trend would then represent a growing probability for trapping moieties to react with ferrocene at rising concentrations generating incrementally purer P3HT.

In order to examine the possibility that ferrocene scavenges traps, time-resolved infrared spectroscopy (TRIR) was employed to investigate polaron lifetimes in thin films spun from Fc:P3HT solutions.[50] TRIR vibrational spectroscopy is capable of resolving IR absorption on ultrafast timescales, allowing direct examination of the dynamics of charge transfer and correlations in polaron recombination.[51] If the addition of ferrocene to P3HT solutions scavenged species that form charge traps, then charge recombination lifetimes of polarons would be expected to be shorter when high ferrocene content solutions are utilized to cast films. The shorter charge recombination lifetimes would appear as faster kinetic decay functions of the transient mid-infrared polaron absorptions. The transient absorption data in **Figure 6** (see also Figure S7, Supporting Information) reveal that the charge recombination lifetimes of P3HT films actually increase with increasing ferrocene content above 25% by mass in solution, a trend that is opposite to what would be expected if ferrocene scavenges species that form charge traps in P3HT. We therefore conclude that ferrocene does not enhance charge carrier mobilities in P3HT films by scavenging species that form charge traps (see further discussion in the Supporting Information). The favorable influence ferrocene has on transport in P3HT films appears to result as or after it is removed from the P3HT films.

Additionally, if a vast reduction in the number of traps was occurring, then confirmation should be available by comparing the hysteresis between forward and reverse I_D–V_G sweeps for neat P3HT and devices from high ferrocene concentration solutions. The large hysteresis commonly reported in OTFT transfer curves has often been attributed to charge trapping within the conduction channel or at the dielectric interface, so fewer charge traps should give rise to a narrower hysteresis.[4,46] This effect has not been observed in our devices (Figure S9, Supporting Information); instead, no significant hysteresis modification was evident with increasing ferrocene content, further indicating the mobility enhancement is not related to ferrocene-induced P3HT purification.

Finally, an experiment designed to decouple potential purification and morphology driven factors was also undertaken. We prepared TFT samples spin coated from neat P3HT, 1:1

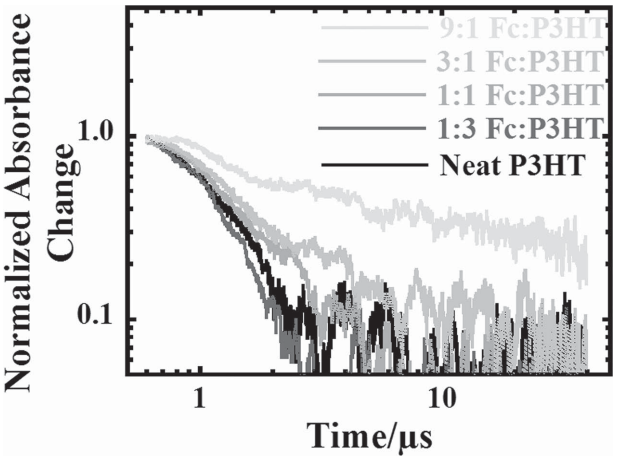

Figure 6. Transient absorption kinetics traces for thin films cast from Fc:P3HT solutions measured by frequency-integrated detection of the mid-IR absorption of polarons in P3HT that remain on the microsecond time scale following 532 nm pulsed excitation.

Fc:P3HT, and 9:1 Fc:P3HT solutions and melted the resulting films at 240 °C for 1 minute prior to quenching at 150 °C for 30 minutes.[52] Melting and quenching, as opposed to annealing, erases crystalline microstructure formed during spin coating. As a result, any mobility enhancement observed during electrical characterization would originate solely from purification effects without the added influence of convoluted morphological parameters. The experiment was performed with films deposited on both trimethoxy(octadecyl)silane (TMOS) and hexamethyldisilazane (HMDS) surface-treated dielectrics, and the results were corroborative. TMOS self-assembled monolayer (SAM) surface-treated dielectrics have demonstrated optimal performance in P3HT devices, but HMDS maintained greater film homogeneity upon melting. Mobilities, as expected, were much lower due to the crystallinity decrease originating in the melting step (Figure S10, Supporting Information), but the general trend indicates charge mobilities remained constant or decreased with increasing ferrocene concentration in solution.[52] These results, combined with the spectroscopy investigation, effectively eliminate charge trap removal as a critical factor and provide further evidence that the mobility enhancement effect is morphology driven.

3. Conclusions

The addition of ferrocene to P3HT casting solutions represents a facile and effective strategy for improving the charge mobilities of polymer devices by roughly a factor of three through strict control of the polymer crystal structure. Our work has shown that source-drain currents and hole mobilities in thin-film transistors increase with increasing ferrocene concentration. The absence of detrimental contact effects, threshold voltage shifts, and changes in hysteresis or off-current levels suggests the use of ferrocene in the described manner does not impair device performance in any capacity. Further investigation revealed the fundamental causes of the observed mobility enhancement were the removal of ferrocene with the solvent during spin coating and the resulting formation of a newly identified polymorph exhibiting a reduced π–π stacking distance.

We have demonstrated that ferrocene influences the self-assembly and morphology of the film. XRD and GIXRD measurements illustrate that the π–π stacking distance decreases without disrupting the packing order of the alkyl side chains by depositing P3HT in the presence of dissolved ferrocene molecules. Prior research into polymer-mediated small molecule polymorphism suggested intimate mixing with weaker intermolecular interactions yields a polymorph with large deviations in the unit cell from that of the neat material. The π-π and hydrophobic interactions between conjugated polymer additives and the small molecule semiconductor during nucleation strongly affected the final polymorph, generating closer stacking and higher charge mobility.[18] In our reverse case, the same effect occurs, but the roles are reversed with the metallocene small molecule inducing the polymorphism of a polymer semiconductor.

With the addition of very high concentrations of ferrocene, charge mobilities of roughly 0.19 $cm^2\ V^{-1}\ s^{-1}$ can be attained in regioregular P3HT under optimal processing conditions. The discovery of new organic semiconductors possessing superior baseline performance has drawn significant interest towards these novel promising materials.[36,53] Consequently, insights gleaned from the analysis of the P3HT/ferrocene system may be successfully applied to the selection and optimization of appropriate polymer/small molecules blends or other additives to further improve charge mobilities in these next generation conjugated polymers. Although the general applicability of our approach to control polymorphism in P3HT is currently unclear, the development of methodologies to control the crystallization of organic semiconductors and maximize device performance may be important for the future disposition of organic components within the electronics market.

4. Experimental Section

Materials: Solutions of highly regioregular poly(3-hexylthiophene-2,5-diyl) (P3HT, 96.3% H-T regioregular, M_w = 77.5 kg mol^{-1}, PDI = 2.0; Lisicon SP001, Merck) and ferrocene (Fc, 99.8%, Acros Organics) or 1,1′-bis(di-tert-butylphosphino)ferrocene (BTBP Fc, 98%, Acros Organics) were prepared in an anhydrous 1,2,4-trichlorobenzene (TCB, ≥99%, Sigma Aldrich) solvent. In the case of P3HT, regioregularity denotes the percentage of stereoregular head-to-tail attachments of the hexyl side chain to the 3 position of the thiophene rings.[22] Similar solutions were also prepared with an alternate polymer semiconductor, poly(2,5-bis(3-hexadecylthiophen-2-yl)thieno[3,2-b]thiophene) (PBTTT, M_w = 82.8 kg mol^{-1}, PDI = 2.68; Lisicon SP210, Merck).[54] Prior research has demonstrated that film inhomogeneity and degradation occurs when spin coating solutions with polymer concentrations below ≈2.5 mg mL^{-1}, so a fixed polymer concentration of 10 mg mL^{-1} was maintained for spin coated TFT samples presented in this report unless otherwise noted.[55] Trichlorobenzene was employed to solvate the polymer, as it has been shown that higher boiling point solvents generated P3HT films with increased crystallinity and generally higher charge mobility.[56,57] Each solution was stirred for approximately 14 hours at room temperature in a nitrogen purged glovebox (MBraun MB Evap and Labmaster Sp). Materials were used as received without additional purification.

Transistor Preparation: Sample bottom-gate, bottom-contact thin-film transistors (TFTs) were prepared using a standard spin casting technique. Heavily doped p-type Si (100) wafers were employed as the gate electrode with a 300 nm thick thermally grown SiO_2 layer serving as the dielectric layer (C = 10.6 nF C^{-1} m^{-2}, Process Specialties, Inc.). Approximately 100 nm thick gold (99.999%, International Advanced Materials) source and drain electrodes were deposited onto the Si/SiO_2 wafers through conventional double-layer lithography techniques at the Penn State Materials Research Institute Nanofabrication Laboratory. High work function gold contacts (≈5 eV) were selected to match the HOMO level of P3HT and other organic semiconductors (≈5–6 eV), thereby minimizing the injection barrier for holes at the source and facilitating extraction at the drain.[11,58] Channel widths and lengths were 220 and 320 μm, respectively, for a W/L aspect ratio of 0.7. Prior to casting, the solution was heated at 90 °C for 1 minute to ensure complete dissolution, and 250 μL of solution was immediately dispensed by pipette onto a trimethoxy(octadecyl)silane (TMOS, 90%, Sigma Aldrich) surface-treated Si/SiO_2 wafer containing gold contact pads. The ≈1 × 1 inch piece of wafer was pre-cleaned with a thorough isopropanol rinse (≥98%, Avantor Performance Materials), UV-ozone scorching (UVO Cleaner Model No. 42, Jelight Co., Inc.) for 20 minutes, an ultrapure DI water rinse (18 MΩ cm, EMD Millipore), and 20 additional minutes of UV-ozone cleaning. The self-assembled monolayer (SAM) surface treatment was applied by immersing the substrate in 16 mL of anhydrous hexadecane (≥99%, Sigma Aldrich) solution containing 20–40 μL of TMOS for approximately 14 hours at room temperature. In certain experiments, a hexamethyldisilazane (HMDS, 99.9%, Sigma-Aldrich) surface treatment

was applied via spin coating at 4000 RPM and soft baking at 90 °C for 90 seconds instead of the TMOS SAM. The SAMs lowered the surface energy of the dielectric and imparted hydrophobicity, removing surface moisture and other polar charge trapping groups at the SiO_2 interface prior to deposition.[43,59] It has also been suggested that the monolayers induce microstructural changes along the interface through specific interactions with functional groups of the polymer to essentially make the polymer "stand up" on its alkyl side chains.[4] After dispensing the polymer solution onto the treated substrate, the liquid was allowed to stand for 40 seconds to wet the surface and promote adhesion before spin casting commenced. Following the allotted wetting period, the active layer was spin cast over the substrate at 1000 RPM for 4 minutes on a spin coater (G3P Spincoat, Specialty Coating Systems Inc.) to remove the solvent and form the film. The as-cast samples were transferred to a calibrated digital hot plate for 3 hours of thermal annealing at 150 °C. Thermal annealing drove off residual solvent and promoted further self-ordering and reorganization of the active layer to increase crystallite thickness.[60] A temperature of 150 °C was selected based on prior optimization studies where the effect of the P3HT annealing temperature was investigated.[52] The samples were rapidly cooled using a metal surface at room temperature, and electrical characterization was performed immediately afterwards with the aid of a probe station (The Micromanipulator Co.) and a Keithley 2636A System Sourcemeter with Kelvin connections to eliminate resistances inherently present in the circuit. All dissolution, spin casting, thermal annealing, and testing was performed without exposing devices to air.

Characterization Methods: The device configurations and environmental conditions used to fabricate the sample TFTs induced p-type behavior in the P3HT active layer. Resultantly, the device gate was swept from positive ("off" state) towards negative biases ("on" state) in order to obtain transfer curve data during characterization. Polarization of the dielectric layer separated positive charges (holes) and negative charges (electrons) within the semiconductor, and the holes collected along the dielectric interface forming an accumulation layer (≈1 nm thick).[12] At the threshold voltage, the gap between the Fermi level of the contacts and the HOMO level of the semiconductor was reduced to the point where hole injection from the source to the active layer occurred, and a conduction channel formed. A voltage applied between the source and drain was then employed to drive the current through the conduction channel via intrachain and interchain charge hopping mechanisms at regions of intermolecular overlapping electron densities (i.e., π–π stacking).[6,11,61] As such, transfer characteristics were acquired by sweeping the gate voltage at a constant source-drain bias of –100 V, and output curves were measured at constant gate biases with source-drain voltage sweeps. Charge carrier mobility, source-drain current, and threshold voltage were the key parameters identified to evaluate the performance of Fc:P3HT devices. Charge mobility can be defined as the ratio between the speed of the charge carriers and the amplitude of the electric field inducing their displacement.[11] The mobility was extracted in the saturation regime from the transfer curve measurements, which exists when the source-drain voltage is greater than the gate voltage minus the threshold voltage. It is generally preferable to extract the mobility from the saturation region because the source-drain current is maximized and nearly independent of source-drain voltage.[6] The channel is "pinched off" because the larger stabilization of the drain potential compared to the gate potential prevents resonance between the Fermi energy and the unoccupied levels and hence the injection of electrons at the drain.[11] Equation (1) was used to extract the hole mobility, where I_D is the current between the source and drain, L and W is the length and width of the channel separating the source and drain, μ is the charge mobility in the active layer, C is the capacitance of the dielectric, V_G is the gate voltage, and V_T is the threshold voltage.[46,47,62,63]

$$I_{D,sat} = \frac{W}{2L}\mu C[V_G - V_T]^2 \quad (V_D > V_G - V_T) \tag{1}$$

Films for time-resolved IR spectroscopy were spin coated directly onto cleaned CaF_2 disks. For normalization purposes, UV–Vis measurements were performed on a Beckman Instruments Single Cell Module DU520 Spectrophotometer to determine the absorbance of each sample at 532 nm. The second harmonic (532 nm) of a pulsed Nd:YAG laser (Surelite I-30, Continuum) operated at 30 Hz, with a pulse duration of ≈8 ns, served as the excitation source for the TRIR experiments.[64] The energy density used was ≈50 μJ cm^{-2}. A compact ceramic globar light source (Spectral Products) was used to generate the IR continuum probe through blackbody emission. The IR probe spectrum was selected using optical filters (2.5 μm cut-on and 10 μm cut-off) because it encompasses the region of polaron absorption in P3HT. After interacting with the region of the sample that was excited by the laser, the IR light was detected by a single element MCT detector (Infrared Associates/Infrared Systems Development). The temporal resolution was determined by the finite carrier lifetime of the MCT detector element and the bandwidth of its 1 MHz pre-amplifier, and the upper limit of the time interval of the instrument, 33 ms, as determined by the laser repetition rate. 30 mg mL^{-1} ^1H NMR solutions were prepared at various ferrocene and P3HT concentrations in deuterated chloroform ($CDCl_3$, 99.8% D, Cambridge Isotope Laboratories, Inc.). Films were also spin coated onto clean 3-inch diameter silicon wafers from Fc:P3HT solutions prepared with TCB in the same manner as described above and redissolved in $CDCl_3$ for NMR analysis. All samples were analyzed with a Bruker Advance 360 Digital NMR at a field strength of 360 MHz. Spin coating, as a casting technique, generated films approximately 50–70 nm in thickness for the stated parameters. Prior studies have suggested that mobility increases when the thickness of the semiconductor film increases.[6] Consequently, film thicknesses were monitored by ellipsometry using a Rudolph Research/AutoEL instrument with a 633 nm wavelength HeNe laser at a fixed angle of 70°, and images of each film were recorded with an optical microscope (Zeiss Neofluar) at 5–50× magnification. X-ray diffraction patterns were obtained for thin films of actual Fc:P3HT and BTBP Fc:P3HT TFTs demonstrating comparable mobilities to those provided in Figure 4. Samples where film quality was good enough for X-ray experiments were used (Fc content in solution at 90% or less). Spectra were obtained using a Rigaku DMAX-Rapid II Microdiffractometer with a Cu Kα source (λ = 1.54 Å) at 50 kV and 40 mA and a 2-dimensional curved image plate detector. Peak positions were identified with 30 minute θ–2θ scans in which the incident beam formed an angle θ (0.25–5°) with respect to the substrate and an angle 2θ (0.5–10°) with the detector. Rocking scans were obtained around the P3HT (100) reflection at q_z = 0.395 $Å^{-1}$ to obtain crystallinity estimates. Samples prepared from Fc:P3HT solutions were rocked between q values of 0.383 and 0.398 $Å^{-1}$ for the 3 hour exposure periods, and BTBP Fc samples were rocked within a q range of 0.385–0.403 $Å^{-1}$ during data acquisition. 2-dimensional scattering profiles with intensity as a function of scattering angle θ and azimuthal angle ω were generated using AreaMax software (Rigaku). The results are provided in Figure S3a and b, where scattering angle was converted to q_z, and intensities were normalized by film thickness. The peak represents the out-of-plane scattering of (100) P3HT lamella stacking, and the degree of crystallinity is proportional to the integral of the rocking curve intensity.[65] As such, the relative crystallinity estimates shown in Figure S3c and d were acquired by integrating the rocking curves in the azimuthal direction and comparing the total peak areas. The P3HT (020) grazing incident wide angle X-ray scattering (GIWAXS) data was obtained on beamline 7.3.3 at the Advanced Light Source, Lawrence Berkeley National Laboratory (λ = 1.24 Å). Samples were prepared by spin coating films from Fc:P3HT and BTBP Fc:P3HT solutions onto TMOS treated silicon and Si/SiO_2 wafers as described above. The wafers were pre-cleaned by sonication in acetone and isopropanol for 10 minutes each followed by 10 minutes of UV-ozone scouring. GIWAXS measurements were taken at angles of 0.15°, 0.175°, and 0.2° which were above the critical angle for P3HT (0.135°) but below the silicon critical angle (0.21°).[56] 2D scattering profiles were reduced from the data using the Nika package for IGOR Pro (Wavemetrics).[66] Solutions for dynamic light scattering analysis were prepared in the same manner as described above for transistor fabrication. Measurements were performed with a Malvern Instruments Nano Series Zetasizer using Zetasizer Software 7.10. The instrument light source was a He-Ne

laser with a wavelength of 633 nm. Optical constants for each Fc:P3HT solution were estimated as weighted averages of the values for neat Fc (n = 1.45, k = 0) and P3HT (n = 1.80, k = 0.085) at 633 nm. The refractive index and absorption coefficient of the 1,2,4-trichlorobenzene dispersant was 1.57 and 0, respectively. Solvent viscosity was taken as 1.61 mPa·s, and the dielectric constant was 2.24.

Supporting Information

UV-Vis analyses of Fc:P3HT solutions and thin films and BTBP Fc:P3HT thin films, results for XPS depth profiling, X-ray scattering experiments, optical micrographs of devices spin coated from high Fc content solutions, DFT-predicted P3HT transfer integrals as a function of Π-stacking distance, a hysteresis comparison for several devices from neat P3HT and 9:1 Fc:P3HT solutions, and average mobilities for drop cast Fc:P3HT transistors and OTFTs from Fc:P3HT solutions after melting and quenching are provided as Supporting Information. This material is available from the Wiley Online Library or from the author.

Acknowledgements

This work was funded by the Center for Flexible Electronics at the Pennsylvania State University and the Dow Chemical Company. The Advanced Light Source is an Office of Science User Facility operated for the U.S. Department of Energy Office of Science by Lawrence Berkeley National Laboratory and supported by the U.S. Department of Energy under Contract No. DE-AC02–05CH11231. The authors also gratefully acknowledge T. Le and C. Guo's assistance with GIXRD measurements, Dr. Y. Lee and P. Zhan's help with NMR measurements, Dr. Kyle Bishop for use of the DLS, and the assistance of the Pennsylvania State University Materials Characterization Laboratory and Nanofabrication Laboratory staff.

Received: September 7, 2014
Revised: October 31, 2014
Published online:

[1] H. Shirakawa, E. J. Louis, A. G. Macdiarmid, C. K. Chiang, A. J. Heeger, *J. Chem. Soc. Chem. Commun.* **1977**, *1*, 578.
[2] a) R. L. Elsenbaumer, K. Y. Jen, R. Oboodi, *Synthetic Metals* **1986**, *15*, 169; b) S. Hotta, S. D. D. V. Rughooputh, A. J. Heeger, F. Wudl, *Macromolecules* **1987**, *20*, 212; c) S. Hotta, M. Soga, N. Sonoda, *Synth. Met.* **1988**, *26*, 267; d) T. A. Chen, R. D. Rieke, *J. Am. Chem. Soc.* **1992**, *114*, 10087; e) R. D. McCullough, R. D. Lowe, *J. Chem. Soc. Chem. Commun.* **1992**, *1*, 70; f) T. Kawase, H. Sirringhaus, R. Friend, T. Shimoda, *SID '01 Digest* **2001**, *40*; g) M. Bjerring, J. S. Nielsen, N. C. Nielsen, F. C. Krebs, *Macromolecules* **2007**, *40*, 6012; h) C. Guo, D. R. Kozub, S. Vajjala Kesava, C. Wang, A. Hexemer, E. D. Gomez, *ACS Macro Letters* **2013**, *2*, 185; i) J. H. Burroughes, D. D. C. Bradley, A. R. Brown, R. N. Marks, K. Mackay, R. H. Friend, P. L. Burns, A. B. Holmes, *Nature* **1990**, *347*, 539; j) L. Kergoat, B. Piro, M. Berggren, G. Horowitz, M. C. Pham, *Anal. Bioanal. Chem.* **2012**, *402*, 1813.
[3] A. Tsumura, H. Koezuka, T. Ando, *Appl. Phys. Lett.* **1986**, *49*, 1210.
[4] H. Sirringhaus, *Adv. Mater.* **2005**, *17*, 2411.
[5] a) A. Gasperini, K. Sivula, *Macromolecules* **2013**, *46*, 9349; b) D. M. DeLongchamp, R. J. Kline, Y. Jung, E. K. Lin, D. A. Fischer, D. J. Gundlach, S. K. Cotts, A. J. Moad, L. J. Richter, M. F. Toney, M. Heeney, I. McCulloch, *Macromolecules* **2008**, *41*, 5709; c) C. Luo, A. K. Kyaw, L. A. Perez, S. Patel, M. Wang, B. Grimm, G. C. Bazan, E. J. Kramer, A. J. Heeger, *Nano Letters* **2014**, *14*, 2764; d) Y. Y. Lin, D. J. Gundlach, S. F. Nelson, T. N. Jackson, *IEEE Electron Device Lett.* **1997**, *18*, 606.
[6] G. Horowitz, *J. Mater. Res.* **2004**, *19*, 1946.
[7] C. P. Jarrett, R. H. Friend, A. R. Brown, D. M. de Leeuw, *J. Appl. Phys.* **1995**, *77*, 6289.
[8] a) H. S. Marsh, O. G. Reid, G. Barnes, M. Heeney, N. Stingelin, G. Rumbles, *J. Polym. Sci. B* **2014**, *52*, 700; b) Y. Mei, M. A. Loth, M. Payne, W. Zhang, J. Smith, C. S. Day, S. R. Parkin, M. Heeney, I. McCulloch, T. D. Anthopoulos, J. E. Anthony, O. D. Jurchescu, *Adv. Mater.* **2013**, *25*, 4352; c) J. Smith, W. Zhang, R. Sougrat, K. Zhao, R. Li, D. Cha, A. Amassian, M. Heeney, I. McCulloch, T. D. Anthopoulos, *Adv. Mater.* **2012**, *24*, 2441.
[9] Y. Diao, L. Shaw, Z. Bao, S. C. B. Mannsfeld, *Energy Environ. Sci.* **2014**, *7*, 2145.
[10] a) A. J. Lovinger, L. J. Rothberg, *J. Mater. Res.* **1996**, *11*, 1581; b) Z. N. Bao, Y. Feng, A. Dodabalapur, V. R. Raju, A. J. Lovinger, *Chem. Mater.* **1997**, *9*, 1299.
[11] J. Cornil, J. L. Brédas, J. Zaumseil, H. Sirringhaus, *Adv. Mater.* **2007**, *19*, 1791.
[12] H. Sirringhaus, M. Bird, N. Zhao, *Adv. Mater.* **2010**, *22*, 3893.
[13] N. D. Treat, M. L. Chabinyc, *Ann. Rev. Phys. Chem.* **2014**, *65*, 59.
[14] Y. D. Park, H. S. Lee, Y. J. Choi, D. Kwak, J. H. Cho, S. Lee, K. Cho, *Adv. Funct. Mater.* **2009**, *19*, 1200.
[15] G. Giri, R. Li, D. M. Smilgies, E. Q. Li, Y. Diao, K. M. Lenn, M. Chiu, D. W. Lin, R. Allen, J. Reinspach, S. C. Mannsfeld, S. T. Thoroddsen, P. Clancy, Z. Bao, A. Amassian, *Nat. Commun.* **2014**, *5*, 3573.
[16] A. Troisi, G. Orlandi, *J. Phys. Chem. B* **2005**, *109*, 1849.
[17] J. Chen, M. Shao, K. Xiao, A. J. Rondinone, Y. L. Loo, P. R. Kent, B. G. Sumpter, D. Li, J. K. Keum, P. J. Diemer, J. E. Anthony, O. D. Jurchescu, J. Huang, *Nanoscale* **2014**, *6*, 449.
[18] J. Chen, M. Shao, K. Xiao, Z. He, D. Li, B. S. Lokitz, D. K. Hensley, S. M. Kilbey, J. E. Anthony, J. K. Keum, A. J. Rondinone, W.-Y. Lee, S. Hong, Z. Bao, *Chem. Mater.* **2013**, *25*, 4378.
[19] A. M. Hiszpanski, S. S. Lee, H. Wang, A. R. Woll, C. Nuckolls, Y. L. Loo, *ACS Nano* **2013**, *7*, 294.
[20] M. Fulem, K. Růžička, C. Červinka, M. Rocha, L. Santos, R. Berg, *J. Chem. Thermodynam.* **2013**, *57*, 530.
[21] T. J. Prosa, M. J. Winokur, J. Moulton, P. Smith, A. J. Heeger, *Macromolecules* **1992**, *25*, 4364.
[22] H. Sirringhaus, P. J. Brown, R. H. Friend, M. M. Nielsen, K. Bechgaard, B. M. W. Langeveld-Voss, A. J. H. Spiering, R. A. J. Janssen, E. W. Meijer, P. Herwig, D. M. de Leeuw, *Nature* **1999**, *401*, 685.
[23] D. T. Duong, V. Ho, Z. Shang, S. Mollinger, S. C. B. Mannsfeld, J. Dacuña, M. F. Toney, R. Segalman, A. Salleo, *Adv. Funct. Mater.* **2014**, *24*, 4515.
[24] a) X. Yu, K. Xiao, J. Chen, N. V. Lavrik, K. Hong, B. G. Sumpter, D. B. Geohegan, *ACS Nano* **2011**, *5*, 3559; b) F. P. V. Koch, J. Rivnay, S. Foster, C. Müller, J. M. Downing, E. Buchaca-Domingo, P. Westacott, L. Yu, M. Yuan, M. Baklar, Z. Fei, C. Luscombe, M. A. McLachlan, M. Heeney, G. Rumbles, C. Silva, A. Salleo, J. Nelson, P. Smith, N. Stingelin, *Prog. Polym. Sci.* **2013**, *38*, 1978; c) G. Gustafsson, O. Inganäs, H. Österholm, J. Laakso, *Polymer* **1991**, *32*, 1574.
[25] L. H. Jimison, M. F. Toney, I. McCulloch, M. Heeney, A. Salleo, *Adv. Mater.* **2009**, *21*, 1568.
[26] J. L. Baker, L. H. Jimison, S. Mannsfeld, S. Volkman, S. Yin, V. Subramanian, A. Salleo, A. P. Alivisatos, M. F. Toney, *Langmuir* **2010**, *26*, 9146.
[27] T. J. Prosa, M. J. Winokur, R. D. McCullough, *Macromolecules* **1996**, *29*, 3654.
[28] Y. Yuan, J. Zhang, J. Sun, J. Hu, T. Zhang, Y. Duan, *Macromolecules* **2011**, *44*, 9341.
[29] M. Brinkmann, P. Rannou, *Macromolecules* **2009**, *42*, 1125.
[30] A. Buono, N. H. Son, G. Raos, L. Gila, A. Cominetti, M. Catellani, S. V. Meille, *Macromolecules* **2010**, *43*, 6772.
[31] C. Poelking, D. Andrienko, *Macromolecules* **2013**, *46*, 8941.

[32] F. P. Koch, M. Heeney, P. Smith, *J. Am. Chem. Soc.* **2013**, *135*, 13699.
[33] G. H. Lu, L. G. Li, X. N. Yang, *Macromolecules* **2008**, *41*, 2062.
[34] M. Brinkmann, *J. Polym. Sci. B Polym. Phys.* **2011**, *49*, 1218.
[35] a) A. Zen, M. Saphiannikova, D. Neher, J. Grenzer, S. Grigorian, U. Pietsch, U. Asawapirom, S. Janietz, U. Scherf, I. Lieberwirth, G. Wegner, *Macromolecules* **2006**, *39*, 2162; b) S. Dag, L. W. Wang, *J. Phys. Chem. B* **2010**, *114*, 5997.
[36] R. Noriega, J. Rivnay, K. Vandewal, F. P. Koch, N. Stingelin, P. Smith, M. F. Toney, A. Salleo, *Nat. Mater.* **2013**, *12*, 1038.
[37] a) H. Sirringhaus, N. Tessler, R. H. Friend, *Synth. Met.* **1999**, *102*, 857; b) D. H. Kim, Y. D. Park, Y. Jang, H. Yang, Y. H. Kim, J. I. Han, D. G. Moon, S. Park, T. Chang, C. Chang, M. Joo, C. Y. Ryu, K. Cho, *Adv. Funct. Mater.* **2005**, *15*, 77.
[38] H. Sirringhaus, *Adv. Mater.* **2014**, *26*, 1319.
[39] G. Giri, E. Verploegen, S. C. Mannsfeld, S. Atahan-Evrenk, H. Kim do, S. Y. Lee, H. A. Becerril, A. Aspuru-Guzik, M. F. Toney, Z. Bao, *Nature* **2011**, *480*, 504.
[40] a) J. L. Bredas, J. P. Calbert, D. A. da Silva, J. Cornil, *Proc. Natl. Acad. Sci. USA* **2002**, *99*, 5804; b) Y. K. Lan, C. I. Huang, *J. Phys. Chem. B* **2008**, *112*, 14857; c) V. Coropceanu, J. Cornil, D. A. da Silva Filho, Y. Olivier, R. Silbey, J.-L. Bredas, *Chem. Rev.* **2007**, *107*, 926.
[41] P. Chen, Q. S. Wu, Y. P. Ding, *Small* **2007**, *3*, 644.
[42] S. S. Lee, C. S. Kim, E. D. Gomez, B. Purushothaman, M. F. Toney, C. Wang, A. Hexemer, J. E. Anthony, Y.-L. Loo, *Adv. Mater.* **2009**, *21*, 3605.
[43] K. Vakhshouri, D. R. Kozub, C. Wang, A. Salleo, E. D. Gomez, *Phys. Rev. Lett.* **2012**, *108*, 26601.
[44] N. D. Treat, J. A. Nekuda Malik, O. Reid, L. Yu, C. G. Shuttle, G. Rumbles, C. J. Hawker, M. L. Chabinyc, P. Smith, N. Stingelin, *Nat. Mater.* **2013**, *12*, 628.
[45] a) M. Manceau, S. Chambon, A. Rivaton, J.-L. Gardette, S. Guillerez, N. Lemaître, *Solar Energy Mater. Solar Cells* **2010**, *94*, 1572; b) S. Fery-Forgues, B. Delavaux-Nicot, *J. Photochem. Photobiol. A* **2000**, *132*, 137; c) J. Worle, A. Ullmann, H. Rost (Polyic GmbH & Co), *US Patent 2009/0001359 A1* **2009**.
[46] E. Orgiu, S. Locci, B. Fraboni, E. Scavetta, P. Lugli, A. Bonfiglio, *Org. Electronics* **2011**, *12*, 477.
[47] L. Bürgi, T. Richards, M. Chiesa, R. H. Friend, H. Sirringhaus, *Synth. Met.* **2004**, *146*, 297.
[48] J. Veres, S. D. Ogier, S. Mohialdin-Khaffaf, S. W. Leeming (Merck GmbH), *US Patent 7 029 945 B2* **2006**.
[49] a) S. P. Gubin, S. A. Smirnova, L. I. Denisovich, A. A. Lubovich, *J. Organomet. Chem.* **1971**, *30*, 243; b) L. M. Mukherjee, *J. Phys. Chem.* **1972**, *76*, 243; c) T. Akiyama, Y. Hoshi, S. Goto, A. Sugimori, *Bull. Chem. Soc. Jpn.* **1973**, *46*, 1851; d) A. M. Bond, F. Scholz, *Langmuir* **1991**, *7*, 3197; e) H. B. Eitouni, N. P. Balsara, H. Hahn, J. A. Pople, M. A. Hempenius, *Macromolecules* **2002**, *35*, 7765; f) S. Haymond, J. K. Zak, Y. Show, J. E. Butler, G. T. Babcock, G. M. Swain, *Anal. Chim. Acta* **2003**, *500*, 137; g) D. A. Durkee, H. B. Eitouni, E. D. Gomez, M. W. Ellsworth, A. T. Bell, N. P. Balsara, *Adv. Mater.* **2005**, *17*, 2003; h) E. I. Rogers, D. S. Silvester, D. L. Poole, L. Aldous, C. Hardacre, R. G. Compton, *J. Phys. Chem. C* **2008**, *112*, 2729.
[50] X. Liu, K. S. Jeong, B. P. Williams, K. Vakhshouri, C. Guo, K. Han, E. D. Gomez, Q. Wang, J. B. Asbury, *J. Phys. Chem. B* **2013**, *117*, 15866.
[51] K. S. Jeong, R. D. Pensack, J. B. Asbury, *Acc. Chem. Res.* **2013**, *46*, 1538.
[52] K. Vakhshouri, E. D. Gomez, *Macromol. Rapid Commun.* **2012**, *33*, 2133.
[53] a) X. Zhang, H. Bronstein, A. J. Kronemeijer, J. Smith, Y. Kim, R. J. Kline, L. J. Richter, T. D. Anthopoulos, H. Sirringhaus, K. Song, M. Heeney, W. Zhang, I. McCulloch, D. M. DeLongchamp, *Nat. Commun.* **2013**, *4*, 2238; b) J. Mei, H. Kim do, A. L. Ayzner, M. F. Toney, Z. Bao, *J. Am. Chem. Soc.* **2011**, *133*, 20130; c) R. Steyrleuthner, R. Di Pietro, B. A. Collins, F. Polzer, S. Himmelberger, M. Schubert, Z. Chen, S. Zhang, A. Salleo, H. Ade, A. Facchetti, D. Neher, *J. Am. Chem. Soc.* **2014**, *136*, 4245.
[54] D. R. Kozub, K. Vakhshouri, S. V. Kesava, C. Wang, A. Hexemer, E. D. Gomez, *Chem. Commun.* **2012**, *48*, 5859.
[55] Y. D. Park, S. G. Lee, H. S. Lee, D. Kwak, D. H. Lee, K. Cho, *J. Mater. Chem.* **2011**, *21*, 2338.
[56] S. V. Kesava, R. Dhanker, D. R. Kozub, K. Vakhshouri, U. H. Choi, R. H. Colby, C. Wang, A. Hexemer, N. C. Giebink, E. D. Gomez, *Chem. Mater.* **2013**, *25*, 2812.
[57] J.-F. Chang, B. Sun, D. W. Breiby, M. M. Nielsen, T. I. Sölling, M. Giles, I. McCulloch, H. Sirringhaus, *Chem. Mater.* **2004**, *16*, 4772.
[58] E. D. Gomez, Y.-L. Loo, *J. Mater. Chem.* **2010**, *20*, 6604.
[59] S. Fabiano, S. Himmelberger, M. Drees, Z. Chen, R. M. Altamimi, A. Salleo, M. A. Loi, A. Facchetti, *Adv. Energy Mater.* **2014**, *4*, 1301409.
[60] a) V. Shrotriya, J. Ouyang, R. J. Tseng, G. Li, Y. Yang, *Chem. Phys. Lett.* **2005**, *411*, 138; b) P. J. Brown, D. S. Thomas, A. Kohler, J. S. Wilson, J. S. Kim, C. M. Ramsdale, H. Sirringhaus, R. H. Friend, *Phys. Rev. B* **2003**, *67*, 64203; c) H. Hintz, H. J. Egelhaaf, L. Lüer, J. Hauch, H. Peisert, T. Chassé, *Chem. Mater.* **2011**, *23*, 145; d) D. R. Kozub, K. Vakhshouri, L. M. Orme, C. Wang, A. Hexemer, E. D. Gomez, *Macromolecules* **2011**, *44*, 5722; e) N. D. Treat, M. A. Brady, G. Smith, M. F. Toney, E. J. Kramer, C. J. Hawker, M. L. Chabinyc, *Adv. Energy Mater.* **2011**, *1*, 82; f) K. Vakhshouri, S. V. Kesava, D. R. Kozub, E. D. Gomez, *Mater. Lett.* **2013**, *90*, 97.
[61] Z. Bao, *Organic Field-Effect Transistors*, CRC Press, Boca Raton **2007**.
[62] A. Bonea, T. Hassinen, B. A. Ofrim, D. C. Bonfert, P. Svasta, *2012 Int. Semiconductor Conf.* **2012**, *2*, 399.
[63] a) D. Gupta, M. Katiyar, D. Gupta, in *Proc. ASID '06,* New Delhi **2006**, 425; b) D. A. Mourey, Ph.D. Thesis, The Pennsylvania State University, **2010**.
[64] R. D. Pensack, K. M. Banyas, J. B. Asbury, *Phys. Chem. Chem. Phys.* **2010**, *12*, 14144.
[65] R. D. Pensack, C. Guo, K. Vakhshouri, E. D. Gomez, J. B. Asbury, *J. Phys. Chem. C* **2012**, *116*, 4824.
[66] a) J. Ilavsky, *J. Appl. Crystallogr.* **2012**, *45*, 324; b) F. Zhang, J. Ilavsky, G. G. Long, J. P. G. Quintana, A. J. Allen, P. R. Jemian, *Metallurg. Mater. Trans. A* **2009**, *41*, 1151.